10038 *Biochemistry* **2009,** *48,* 10038–10046
DOI: 10.1021/bi901093w

BIOCHEMISTRY
including biophysical chemistry & molecular biology
Article

Intrinsic Dynamics in ECFP and Cerulean Control Fluorescence Quantum Yield[†]

Mickaël Lelimousin,[‡,∥] Marjolaine Noirclerc-Savoye,[‡,∥] Christelle Lazareno-Saez,[‡,∥] Bernhard Paetzold,[§] Sophie Le Vot,[‡] Richard Chazal,[‡] Pauline Macheboeuf,[‡] Martin J. Field,[‡] Dominique Bourgeois,[‡,§] and Antoine Royant*[,‡,§]

[‡]*Institut de Biologie Structurale Jean-Pierre Ebel, UMR 5075 CNRS-CEA-Université Joseph Fourier, 41 rue Jules Horowitz, F-38027 Grenoble Cedex 1, France, and* [§]*European Synchrotron Radiation Facility, 6 Rue Jules Horowitz, BP 220, F-38043 Grenoble Cedex, France.* [∥]*These authors equally contributed to the work.*

Received June 29, 2009; Revised Manuscript Received September 14, 2009

ABSTRACT: Enhanced cyan fluorescent protein (ECFP) and its variant Cerulean are genetically encoded fluorophores widely used as donors in FRET-based cell imaging experiments. First, we have confirmed through denaturation experiments that the double-peak spectroscopic signature of these fluorescent proteins originates from the indole ring of the chromophore. Then, to explain the improvement in the fluorescence properties of Cerulean compared to those of ECFP, we have determined the high-resolution crystal structures of these two proteins at physiological pH and performed molecular dynamics simulations. In both proteins, the N-terminal half of the seventh strand exhibits two conformations. These conformations both have a complex set of van der Waals interactions with the chromophore and, as our simulations suggest, they interconvert on a nanosecond time scale. The Y145A and H148D mutations in Cerulean stabilize these interactions and allow the chromophore to be more planar, better packed, and less prone to collisional quenching, albeit only intermittently. As a consequence, the probability of nonradiative decay is significantly decreased. Our results highlight the considerable dynamical flexibility that exists in the vicinity of the tryptophan-based chromophore of these engineered fluorescent proteins and provide insights that should allow the design of mutants with enhanced optical properties.

The potential of green fluorescent protein (GFP)[1] to be a genetically encoded fluorescent reporter was demonstrated as early as 1994 (*1*). The chromophore results from the autocyclization of three consecutive amino acid residues (serine-tyrosine-glycine) located inside the β-barrel-shaped core of the protein. Efforts to tune the color of its emission by random and site-directed mutagenesis enlarged its palette to blue, cyan, and yellow (*2*). Mutation of the chromophore's tyrosine into a tryptophan was crucial in obtaining the cyan fluorescent protein ECFP (Figure 1a), and yellow fluorescence was achieved in EYFP by positioning a second tyrosine in a π-stacking interaction with the tyrosine of the chromophore. The spectral overlap between ECFP and EYFP has made it an attractive pair for the development of genetically encoded FRET sensors (*3*). As a result, ECFP has become a popular reporter but with nonideal spectroscopic properties: its brightness is significantly lower than those of most other widely used fluorescent proteins (*4*), its excitation and emission fluorescence spectra are two-peaked and broad, and its fluorescence lifetime behavior is multiexponential (*5*).

Several groups have tried to optimize the spectroscopic properties of ECFP. CyPet was obtained by an evolutionary strategy, with the sole constraint of optimizing the FRET signal to a yellow FP (*6*). Rational design was possible only after the crystal structure of ECFP had been determined (*7*). Inspection of the structure revealed the presence of two alternate conformations of the [144−149] strand, one very close to the one adopted in GFP with the Tyr145 side chain in the vicinity of the chromophore (conformation A or *gfp*, PDB entry 1OXD, green trace in Figure 1b) and a new conformation in which Tyr145 points toward the bulk solvent (conformation B or *ecfp*, PDB entry 1OXE, cyan trace in Figure 1b). This supports the observation from ^{19}F NMR experiments that the chromophore interconverts between two conformations on the millisecond time scale (*8*). As Tyr145 and His148 interact either with the solvent or with the chromophore in each conformation, it was postulated that these residues modulate the fluorescence properties of the protein (*9*). The S72A/Y145A/H148D triple mutant, called Cerulean, was shown to exhibit a significant increase in brightness and a reduced heterogeneity of fluorescence lifetimes (*9*−*11*). The structure of Cerulean was recently determined at pH 5.0, showing an unanticipated *E* configuration of the C_β−C_γ bond of the chromophore (*12*). However, the differences in experimental conditions, most importantly in pH, make the identification of the reasons for fluorescence improvement very difficult, underscoring the need for a structure of Cerulean at a higher pH.

[†]Support by the Agence Nationale de la Recherche (ANR-07-BLAN-0107-01) is acknowledged.

*To whom correspondence should be addressed. E-mail: antoine.royant@ibs.fr. Telephone: (+33) 4 38 78 96 28. Fax: (+33) 4 38 78 54 94.

[1]Abbreviations: FRET, Förster resonance energy transfer; MD, molecular dynamics; QY, fluorescence quantum yield; VdW, van der Waals; ECFP, enhanced cyan fluorescent protein; EGFP, enhanced green fluorescent protein; CFP, cyan fluorescent protein; GFP, green fluorescent protein; H-bond, hydrogen bond; FP, fluorescent protein; T_m, melting temperature; rms, root-mean-square; conf, conformation; PEG, polyethylene glycol; RI, refractive index; TCSPC, time-correlated single-photon counting; EC, extinction coefficient; QC/MM, quantum chemistry/molecular mechanics; PDDG-PM3, Pairwise Distance-Directed Gaussian-Parametric Method 3; [10,10]-CISD, singly and doubly excited configuration interaction method within an active space of 10 electrons and 10 molecular orbitals; OPLS-AA, optimized potential for liquid simulations, all atoms; PDB, Protein Data Bank.

 Published on Web 09/15/2009

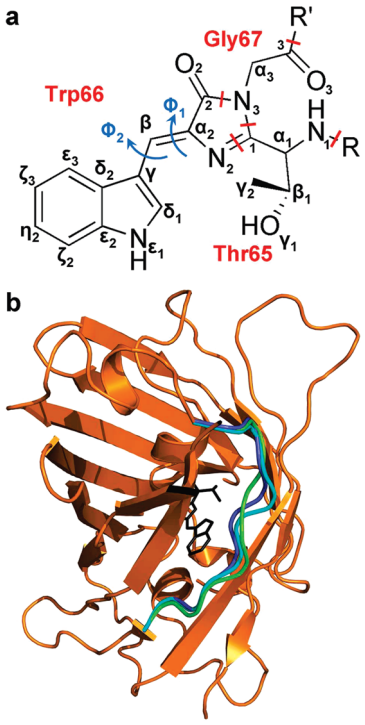

FIGURE 1: (a) Schematic representation of the chromophore in ECFP and Cerulean with atom numbering. R and R′ correspond to residues Leu64 and Val68, respectively. Red lines delimit individual amino acid residues within the chromophore. Dihedral angles Φ_1 and Φ_2 around the aryl−alkene bond are colored blue. (b) Representation of ECFP's three-dimensional structure in gold as determined in this study. The main chain trace of the [141−151] strand of its *ecfp* conformation is colored cyan. For the sake of comparison, the *gfp* and *cerulean* conformations of the strand are colored green and deep blue, respectively, as they are observed in the structures of EGFP (*15*) and Cerulean (this study). All figures were prepared with PyMol (DeLano Scientific).

In this work, we report the crystal structures of ECFP and Cerulean under physiological pH crystallization conditions at 1.37 and 1.15 Å resolution, respectively. We have also performed fluorescence measurements (emission spectra and lifetimes) on crystals to ensure that the spectroscopic properties were preserved in the crystal, and that the structures reflect the properties they have in solution. The high degree of similarity between the structures of ECFP and Cerulean prompted us to undertake a molecular dynamics simulation study to analyze the differences in chromophore interactions, in particular with residues 143−150 of the seventh strand. We were able to identify a structural determinant for the improved quantum yield (QY) of Cerulean. Altogether, our results give a highly dynamic picture of the interaction between the chromophore and its protein matrix.

MATERIALS AND METHODS

Molecular Biology. ECFP cDNA in the pQE expression vector (Qiagen) was a kind gift from Prof. N. Budisa. The different mutants were obtained sequentially from ECFP by Quick change mutagenesis. ECFP-Y145A/H148D was obtained from ECFP with the following primers: Y145A/H148D_For, 5′-CTGGAGTACAACGCCATCAGCGACAACGTCTATATCACCG-3′; Y145A/H148D_Rev, 5′-CGGTGATATAGACGTTGTCGCTGATGGCGTTGTACTCCAG-3′. Cerulean was obtained from ECFP-Y145A/H148D with the following primers: S72A_For, 5′-CGTGCAGTGCTTCGCCCGCTACCCCGAC-3′; S72A_Rev, 5′-GTCGGGGTAGCGGGCGAAGCACTGCACG-3′. All constructs were confirmed by DNA sequencing.

Expression and Purification. His-tagged recombinant proteins were expressed in *Escherichia coli* BL21 CodonPlus (DE3) RIL cells (Stratagene) in autoinduction medium (*13*), at 27 °C for 24 h. Cells were lysed by sonication in the presence of 20 mM Tris (pH 8) and 500 mM NaCl with EDTA-free protease inhibitors (Complete, Roche). His-tagged proteins were purified on a Ni-NTA Superflow column (Qiagen) and eluted with 100 mM imidazole in the buffer described above. Fractions containing purified proteins were pooled, dialyzed against 20 mM Tris (pH 8.0), and concentrated to 25−70 mg/mL.

Thermal Shift Assay. Assays were performed using an IQ5 96-well format real-time PCR detection system (Bio-Rad) over the temperature range of 20−100 °C at a rate of 1 °C/min. Assay samples were prepared with 23 μL of protein (2 mg/mL) and 2 μL of 250× SYPRO Orange dilution (Molecular Probes) in a 96-well thin-wall PCR plate (Bio-Rad). The plates were heated, and changes in fluorescence for the environmentally sensitive dye SYPRO Orange were monitored through a charge-coupled device (CCD) camera (*14*). The melting temperature (T_m) values of each protein were determined graphically from the fluorescence first derivative of the melting curves. The wavelengths for excitation and emission were 470 and 570 nm, respectively.

Crystallization. We obtained diffraction-quality crystals under conditions based on those published for ECFP and EGFP (*7*, *15*). Crystals were grown from a protein solution at 12−20 mg/mL in 0.1 M Hepes (pH 6.7−7.5), 14−20% PEG8000, and 0−0.1 M $MgCl_2$ in 1−1.5 μL hanging drops using the vapor diffusion method. Crystals were transferred to a cryoprotectant solution consisting of the mother liquor supplemented with 20% (v/v) glycerol.

Structure Determination. X-ray diffraction data were collected at 100 K on macromolecular crystallography beamlines ID14-eh1 and ID29 of the European Synchrotron Radiation Facility and processed using XDS (*16*). All crystals belong to the $P2_12_12_1$ space group. The solvent content is 40%. A 5% random set of reflections was selected for R_{free} flagging for the first ECFP data set and kept for each subsequent data set. Structure refinement was conducted with Refmac (*17*). Structures have been deposited in the Protein Data Bank as entries 2WSN for ECFP and 2WSO for Cerulean. Crystallographic data statistics can be found in Table S1 of the Supporting Information.

Spectroscopic Characterization. Absorption spectra of solution samples were measured on a UV−visible spectrophotometer (Cary 3E, Varian). Extinction coefficients were obtained by a method derived from the one used for tyrosine-containing GFP chromophores (*18*). Protein samples with an optical density not higher than 0.7 were denatured by addition of an equal volume of 1 M NaOH. The method relies on knowledge of the absorption properties of a tryptophan-based chromophore, free from its protein environment, which is missing in the literature. We used 30 mM^{-1} cm^{-1} as an average of the published values of EC_{434} of ECFP. EC for the denatured chromophore was then deduced to be 46 mM^{-1} cm^{-1} at 462 nm (Figure S1 of the Supporting Information). Fluorescence emission spectra of protein samples were measured on a fluorimeter (Fluorolog 3, HORIBA Jobin Yvon). Fluorescence quantum yields were calculated on protein samples with an optical density not higher than 0.05, using 9-aminoacridine as a standard (QY = 0.97 in water). Finally, the overall level of fluorescence can be quantified

Table 1: Spectroscopic and Biochemical Characterization of ECFP Mutants

	ECFP	ECFP-Y145A/H148D	Cerulean
absorption maximum (nm)	435	434	434
molecular extinction coefficient (mM^{-1} cm^{-1})	30.0 ± 0.4 (n = 6)[a]	30.2 ± 0.3 (n = 4)	30.7 ± 0.3 (n = 5)
emission maximum (nm)	474	474	474
quantum yield	0.30 ± 0.01 (n = 6)	0.44 ± 0.01 (n = 10)	0.44 ± 0.01 (n = 8)
brightness	9.0	13.4	13.7
average fluorescence lifetime in solution (ns)	3.2 ± 0.1 (n = 23)	3.7 ± 0.2 (n = 6)	3.8 ± 0.2 (n = 5)
average fluorescence lifetime in crystal (ns)	2.2 ± 0.2 (n = 3)	2.8 ± 0.3 (n = 3)	2.7 ± 0.4 (n = 7)
denaturation temperature (°C)	75.7 ± 0.1 (n = 3)	82.0 ± 0.4 (n = 3)	85.3 ± 0.4 (n = 3)

[a] n is the number of individual measurements.

by brightness, the product of the extinction coefficient and the quantum yield.

Absorption and fluorescence emission spectra for crystals were recorded at the Cryobench laboratory of the European Synchrotron Radiation Facility (*19*). Fluorescence lifetime measurements were performed using a time-correlated single-photon counting (TCSPC) setup adapted for crystals and solutions at either cryogenic or room temperature, with an excitation wavelength of 440 nm and a 470 nm interferential emission filter, and a time resolution of ~230 ps (*19*).

Molecular Dynamics Simulations. MD simulations were performed on the *ecfp* conformation of ECFP and the *ecfp* and *cerulean* conformations of Cerulean that were obtained by X-ray crystallography. The fDynamo library (*20*) was used to set up the systems and to analyze the MD trajectories. Simulations were conducted with AMBER 9 (University of California, San Francisco, CA), applying the OPLS-AA force field to the protein (*21*) and the TIP3P water model to the solvent (*22*). Parameters for the chromophore were deduced from equivalent groups in the OPLS-AA force field and were similar to those previously used in the literature (Appendix 1 of the Supporting Information) (*23*). Protonation states for the proteins at pH 7 were estimated using pK_a calculations (*24*). The resulting structures were then solvated in cubic boxes of water molecules, and sufficient cations were added to ensure a total system charge of zero using SODIUM (Beckman Institute). Langevin molecular dynamics simulations with a duration of 39 ns were performed for each system at constant pressure (1 atm) and temperature (300 K). A detailed description of the protocol is provided as Supporting Information (Paragraph S1). Coordinates were saved every 2 ps, resulting in 19500 structures per simulation, and all results presented in this article are based on this sampling. Snapshots of the molecular dynamics simulations superimposed on the X-ray structures, as well as root-mean-square deviations on C_α positions between simulated and X-ray structures, are reported as Supporting Information for the sake of illustration (Figure S2).

Electron density comparisons between S_0 and S_1 states were conducted with the fDynamo library (*20*) using a hybrid quantum chemical/molecular mechanical (QC/MM) potential (*25*). The PDDG-PM3 semiempirical method (*26*) was employed in conjunction with a standard configuration interaction method ([10,10]-CISD) to calculate the wave function on the chromophore. Remaining atoms were treated with the OPLS-AA force field.

RESULTS

The aim of our study is to provide an explanation for the improvement of the fluorescence properties of Cerulean compared to those of ECFP. Given the significant discrepancy in reported values (*9*, *10*), we have redetermined molar extinction coefficients (ECs) and quantum yields (QYs) for ECFP, ECFP-Y145A/H148D, and Cerulean (Table 1) to allow for an accurate comparison. ECs are indistinguishable, whereas the QYs of ECFP-Y145A/H148D and Cerulean are ~50% higher than that of ECFP. Fluorescence lifetime measurements show that each protein displays two lifetimes, and the average fluorescence lifetime increases by ~20% between ECFP and the other two mutants, reflecting the fluorescence QY improvement. Overall, this shows that the S72A mutation has no effect on the spectroscopic properties, and our structural study will focus on the Y145A and H148D mutations to explain QY modulation.

We recorded absorption and fluorescence spectra on all mutant crystals, and measured their fluorescence lifetimes, to determine whether the crystal environment affects the spectroscopic properties of the protein at room temperature. Fluorescence emission spectra and TCSPC histograms can be found as Supporting Information (Figures S3 and S4). The positions of the absorption and emission peaks are conserved, whereas the fluorescence lifetimes show a ~25% decrease. This can be explained by the difference in the refractive index of the medium surrounding the protein (*27*). The refractive index (RI) of water is 1.33; a salt crystal has a RI of 1.54, and a lysozyme crystal can have a RI as high as 1.45 (*28*). Overall, this indicates that spectroscopic properties are fairly well conserved on going from dilute solution to the concentrated arrangement of molecules in the crystal at room temperature and that the information derived from our structural analyses should be relevant in explaining differences between mutants.

We wanted to determine whether the mutations of Cerulean were beneficial to the thermal stability of the protein. Using the thermal shift assay, we indeed observed a gradual increase in the melting temperature (T_m) from ECFP to Cerulean with the sequential additions of Y145A/H148D and S72A double and single mutations (Table 1). Interestingly, we found a similar correlation with the resistance to denaturation in NaOH during EC measurements. Denaturation was immediate for ECFP and ECFP-Y145A/H148D and complete after 3 min for Cerulean, highlighting the stabilizing role of the S72A mutation.

Because we anticipated that accurate determination of the [143−150] strand structure would be fundamental to our study (*7*), we devised a specific procedure for the first steps of the ECFP structure determination process. Phases were obtained by molecular replacement using a partial model of the published structure of ECFP based on a common core identical to the *gfp* and *ecfp* conformations (*7*). This model excluded the chromophore, the complete strand from residue 143 to 150, all water molecules, and the side chains of Ser205, Ile220, and Glu222.

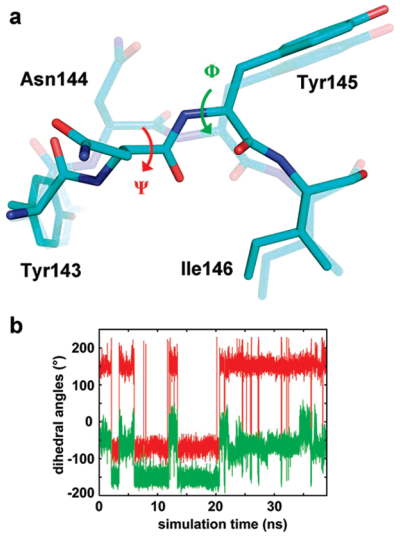

FIGURE 2: (a) Representation of residues 143−146 in the *ecfp* (solid cyan) and *ecfp*′ (transparent cyan) conformations of the crystal structure of ECFP. Dihedral angles Ψ and Φ are defined on each side of the Asn144−Tyr145 peptide bond. In the crystal structure of ECFP, Ψ = 161.6° and Φ = −54.3° for the *ecfp* conformation, Ψ = −71.9° and Φ = −152.9° for the *ecfp*′ conformation. (b) Evolution of Ψ (red trace) and Φ (green trace) during the molecular dynamics simulation starting from the *ecfp* conformation of ECFP showing that it transiently adopts the *ecfp*′ conformation.

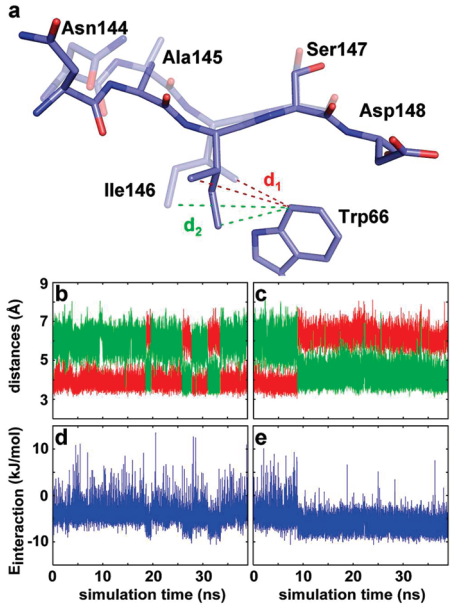

FIGURE 3: (a) Representation of residues 66 and 144−148 in the *cerulean* (solid blue) and *ecfp* (transparent blue) conformations of the crystal structure of Cerulean. Distances d_1 and d_2 between Trp66 atom $C_{\zeta 2}$ and either atom $C_{\gamma 2}$ or atom $C_{\delta 1}$ of Ile146 are colored red and green, respectively. Evolution of d_1 (red) and d_2 (green) during molecular dynamics simulations started from the *ecfp* X-ray conformations of ECFP (b) and Cerulean (c). These distances served to monitor the *ecfp* ↔ *ecfp*″ and *ecfp* ↔ *cerulean* transitions in ECFP and Cerulean, respectively. d_1 = 3.9 Å and d_2 = 5.8 Å for the *ecfp* conformation in the crystal structure of ECFP; in the crystal structure of Cerulean, d_1 = 3.9 Å and d_2 = 5.9 Å for the *ecfp* conformation and d_1 = 6.0 Å and d_2 = 3.7 Å for the *cerulean* conformation. (d and e) Interaction energy terms between Trp66 and Ile146's side chain for ECFP (d) and Cerulean (e). This shows that the *ecfp*″ or *cerulean* conformation of Ile146 is in a better interaction with the chromophore in both ECFP and Cerulean, resulting in a significantly lower probability of collisional quenching.

After initial positional refinement, good quality electron density was interpretable for the chromophore, all side chains, and most of the [143−150] strand. At first glance, the strand appeared to be in a single conformation that closely resembles the *ecfp* conformation. However, the electron density was significantly weaker between main chain atoms C and C_α of Asn144 (Figure S5a). Because such a cleavage of the main chain is unlikely, we investigated the possibility of dual conformations at this position and indeed found that putting residues 143−146 in alternate conformations explained the weakened electron density at this position (Figure S5a and Figure 2a). The two conformations of ECFP in our crystal structure were denoted *ecfp* (cyan trace in Figure 1b) and *ecfp*′. Both clearly differ from the previously observed *gfp* conformation (green trace in Figure 1b) (*7*), which we were unable to unambiguously identify in our crystals. We hypothesize that its absence originates from the significantly larger amount of PEG in our crystallization conditions, resulting in a more viscous mother liquor.

We used the same protocol to determine the structure of Cerulean, which is very close to that of ECFP. The main difference is found on the [143−150] strand, which could also be rebuilt in two alternate conformations (Figure S5b and Figure 3a), one closely resembling the *ecfp* conformation ("Outside" conformation of the main chain) and a new one in which the main chain is closer to the chromophore ("Inside" conformation of the main chain) (blue trace in Figure 1b). These two conformations are called *ecfp* and *cerulean*, respectively. In the latter conformation, the side chain of Ile146 adopts a new conformation (Figure S5d) that is closer to the chromophore than in the *ecfp* conformation (Figure 4 and Figure S5c).

In both ECFP and Cerulean, the chromophore is in the *Z*,*Z* configuration at physiological pH when the two partial $C_{\alpha 2}-C_\beta$ and $C_\beta-C_\gamma$ double bonds are considered (Figure S5c,d). Its conformation is controlled by the surrounding amino acid residues, mostly through van der Waals (VdW) interactions (Figure 4). A detailed description of the interactions between

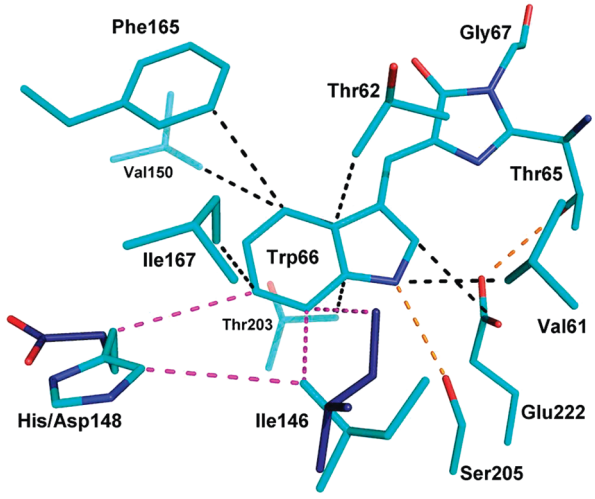

FIGURE 4: Environment of the indole ring of the chromophore in ECFP and Cerulean. The main two H-bonds stabilizing the chromophore are colored orange. Distances shorter than 4.0 Å illustrating potential VdW interactions are colored black. The critical set of VdW interactions among Trp46, Ile146, and His148 is colored purple. The two residues in Cerulean showing a different interaction with the chromophore, Ile146 and Asp148, are colored deep blue.

the protein and its chromophore can be found as Supporting Information (Paragraph S2). The sole difference in chromophore environment between ECFP and Cerulean is in the orientation of

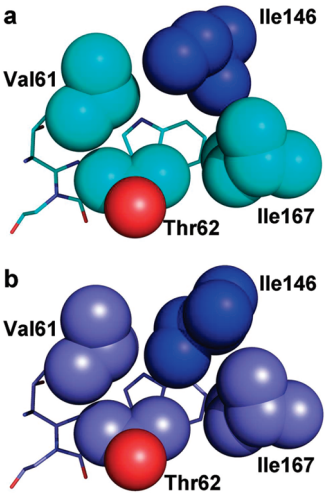

FIGURE 5: Comparison of the chromophore environment around Ile146 in ECFP and Cerulean. Atoms are depicted as spheres with their VdW radii. (a) In ECFP, Ile146 is clearly distant from Thr62, leaving an empty cavity in the immediate vicinity of the chromophore. (b) Ile146 in the *cerulean* conformation of Cerulean. The complementarity of the Ile146 side chain to those of Val61, Thr62, and Ile167 indicates that these four residues form VdW interactions and provide an enhanced stabilization to the chromophore, which is supported by energy calculations.

Table 2: Torsion Angles of the Chromophore in CFPs and Other Fluorescent Proteins

	ECFP	Cerulean	GFP	Citrine	DsRed	Rtms5
PDB entry	2WSN	2WSO	1W7S	1HUY	1G7K	1MOV
QY	0.30	0.44	0.67	0.71	0.68	0.00
Φ_1[a] (deg)	6.6	5.3	0.2	0.8	0.9	−11.5
Φ_2[a] (deg)	−6.8	−6.4	−0.2	−0.4	0.1	42.4

[a] Φ_1 and Φ_2 are chromophore torsion angles around the $C_{\alpha 2}-C_\beta$ and $C_\beta-C_\gamma$ bonds.

residues 146 and 148. In Cerulean, Asp148 is exposed to the solvent, whereas in ECFP the side chain of His148 is parallel to the surface of the protein, allowing it to be within VdW interaction distance of Ile146. The latter residue has a peculiar position in the *cerulean* conformation of Cerulean (Figure 3a), as it interacts preferentially with Val61, Ile167, and Thr203, thereby producing a tighter packing (Figure 5). The chromophore is clamped by two pairs of residues that are largely responsible for preventing rotation of the indole ring with respect to the imidazolinone (Paragraph S2). The degree of chromophore planarity can be estimated by inspection of the values of the torsion angles Φ_1 and Φ_2 about the $C_{\alpha 2}-C_\beta$ and $C_\beta-C_\gamma$ bonds, both of which have partial double-bond character (Figure 1a). As a result of the clamping, the chromophore is roughly planar, albeit only approximately when compared to the parent GFP and DsRed (*29*), and is slightly more planar in Cerulean than in ECFP (Table 2).

Although we identified a slightly different interaction between the protein and the chromophore in the crystal structures of ECFP and Cerulean, we could only hypothesize that the change in orientation of Ile146 and residue 148 would explain the improvement in QY (Figure 4). We postulated that molecular dynamics simulations based on our structures could unveil subtle details of the interactions between the chromophore and the protein matrix. Three molecular dynamics simulations 39 ns in duration were performed starting from the X-ray structures of ECFP in the *ecfp* conformation and Cerulean in both the *ecfp* and *cerulean* conformations. We did not expect the conversion of any of our structures to the *gfp* conformation, since the *ecfp* to *gfp* conversion should occur on the millisecond time scale (*8*). During the ECFP simulation, frequent switching between the *ecfp* and *ecfp′* conformations is observed (Figure 2b), but this local variation of dihedral angles between C_α atoms of Asn144 and Tyr145 is not correlated with significant changes in other residue interactions. Unexpectedly, a new conformation, *ecfp″*, is transiently observed (Figure 3b and Movie S1 of the Supporting Information), in which Ile146 adopts its *cerulean* conformation and the main chain of residues 143−150 its *ecfp* (or Outside) conformation (Table 3). For Cerulean, the *cerulean* conformation is preserved throughout the 39 ns simulation, whereas the *ecfp* conformation converts to the *cerulean* one after only 9 ns (Figure 3c and Movie S2 of the Supporting Information), thereby suggesting that the *cerulean* conformation is the more stable one. A scheme summarizing the conformations adopted by ECFP and Cerulean is depicted in Figure 6. Averaging energy terms between pairs of residues 66, 146, and 148 over the course of the simulation demonstrates that these three residues are engaged, on average, in cooperative attractive VdW interactions in ECFP (Table 3). The situation is markedly different in Cerulean as such a three-partner interaction does not exist: there is a repulsive electrostatic energy term between Trp66 and Asp148, hardly any interaction between Ile146 and Asp148, and a strong VdW interaction between Trp66 and Ile146.

Monitoring of torsion angles during the molecular dynamics simulations shows that the chromophore retains a slightly twisted conformation in ECFP, and an almost perfectly planar conformation in Cerulean (Table 3). We have observed that the probability of a positive Trp66−Ile146 interaction energy is much higher in the *ecfp* conformation than in the *ecfp″* and *cerulean* conformations; i.e., it occurs when Ile146 interacts via its $C_{\gamma 2}$ atom with the chromophore (Table 3 and Figure 3d,e). VdW interactions with positive energy correspond to a situation in which atoms that are too close repel each other. This implies that in the *ecfp* conformation, the chromophore of ECFP or Cerulean has a higher probability of undergoing a molecular collision event with Ile146. In contrast, the conformation of Ile146 in *ecfp″* and *cerulean* favors a cohesive interaction with the chromophore (Table 3 and Figure 3d,e). Finally, we have analyzed the interaction of Ile146 with the residues forming the binding pocket on one side of the chromophore's indole ring, namely, Val61, Ile167, and Thr203 (Figure 5). These residues engage in VdW interactions that are 2 kJ/mol more stabilizing in Cerulean than in ECFP when equivalent conformations are compared. In addition, Ile146 interacts more strongly with either Trp66 or the Val161-Ile167-Th203 set in the *ecfp″* and *cerulean* conformations, suggesting a cooperative effect (Table 3).

Our simulations were performed with a chromophore in its ground state. To test if the results could be relevant to the situation when the chromophore is in an excited state, we have calculated the differences in electron density on the chromophore between the ground and excited states at several time points of the simulations (Appendix S2 of the Supporting Information). Differences were observed to be restricted to the imidazolinone ring and the methylene bridge. As a consequence, we postulate that the electrostatic interactions between the [143−150] strand and the indole ring of the chromophore should be comparable between the ground and excited states. Moreover, since the interactions between the strand and the indole ring are essentially

Table 3: Statistics from MD Simulations of the Observed Conformations of ECFP and Cerulean[a]

	ECFP		Cerulean	
	ecfp	*ecfp″*	*ecfp*	*cerulean*
conformation of the [143−150] strand	Outside	Outside	Outside	Inside
$\langle E_{I146-res148} \rangle$ (kJ/mol), type	−1.6 (1.0), VdW	−1.8 (1.2), VdW	−0.5 (0.8), both	−0.1 (0.3), both
$\langle E_{I146-3AA} \rangle$ (kJ/mol), type	−8.3 (1.9), VdW	−8.7 (2.1), VdW	−9.5 (3.1), VdW	−10.5 (2.7), VdW
$\langle E_{I146-W66} \rangle$ (kJ/mol), type	−4.0 (1.6), VdW	−6.0 (1.7), VdW	−4.4 (1.9), VdW	−6.4 (1.7), VdW
probability of $E_{I146-W66} > 0$ (‰)	21	3	28	1
$\langle E_{W66-res148} \rangle$ (kJ/mol), type	−1.5 (1.6), VdW	−2.4 (1.6), VdW	8.3 (1.4), elec	8.0 (1.1), elec
$\langle \Phi_1 \rangle$ (deg)	−8.8 (9.8)	−11.1 (9.6)	−1.6 (9.5)	−0.7 (10.5)
$\langle \Phi_2 \rangle$ (deg)	−1.4 (6.5)	−1.4 (6.5)	0.7 (6.4)	0.6 (6.5)

[a]The three sections, from top to bottom, refer to parameters relevant to the conformation of Ile146, the interaction between Ile146 and Trp66, and chromophore planarity, respectively. $\langle E_{res1-res2} \rangle$ is the mean interaction energy between residues 1 and 2. VdW, van der Waals interactions; elec, electrostatic interactions; 3AA, Val61, Ile167, and Thr203. The values in parentheses refer to the standard deviations of the mean.

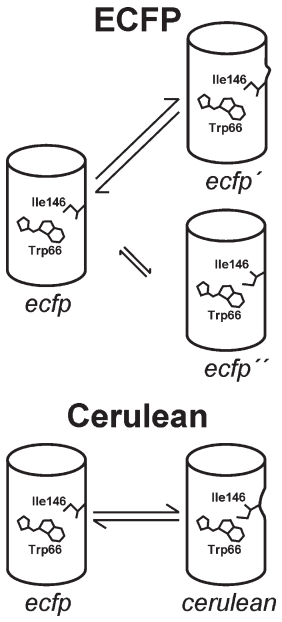

FIGURE 6: Schematic representation of conformations *ecfp*, *ecfp′*, *ecfp″*, and *cerulean* adopted by ECFP and Cerulean. Deformation of the cylinder indicates the conformation of the [143−150] strand with respect to the chromophore. Ile146 adopts one of two conformations with respect to the chromophore in each conformation. Conversion from one conformation to the other probably happens on a nanosecond time scale. The infrequency of the *ecfp″* conformation is denoted by the shorter equilibrium arrows.

of van der Waals nature, the whole set of interactions must be globally conserved.

DISCUSSION

In this study, we have attempted to relate the structures of tryptophan-based chromophore fluorescent proteins to their spectroscopic properties. ECFP is well-known for having two peaks in its absorption, fluorescence excitation, and emission spectra, and several hypotheses have been put forward to explain this. In particular, it was proposed that it could be due to different structures of the protein (*7*), but it has been more recently suggested that this is in fact an intrinsic property of tryptophan-based chromophores (*12*). The latter hypothesis is in agreement with the spectroscopic characteristics of Honeydew, a yellow-green fluorescent protein derived from the red FP DsRed, which harbors a tryptophan-based chromophore in a very different amino acid residue environment compared to that of ECFP (*29*, *30*). In addition, we observe in our NaOH-driven denaturation experiments that the chromophore, most likely freed from its specific interactions with the protein, retains two peaks in its absorption spectrum (Figure S1). This constitutes an additional piece of evidence that this is a feature of tryptophan-based chromophores, which will not be eliminated by any set of mutations.

The critical mutation that gives ECFP its cyan light emission property is Y66W as this mutation alone suffices to turn enhanced green fluorescent protein (EGFP) into a CFP, although with a low level of fluorescence. The optimized ECFP contains the three additional mutations, N146I, M153T, and V163A, all found close to the chromophore, and presumably necessary for accommodating the increased bulk of the indole ring when compared to the tyrosyl group of GFP (*31*). Since M153T and V163A changes are present in other well-known green and yellow mutants such as Emerald, GFPuv, or Venus, it is apparent that the replacement of a hydrophilic residue with a hydrophobic residue in the N146I mutation plays a pivotal role. In wild-type GFP, Asn146's side chain is completely exposed to the solvent and Tyr145 is buried in the vicinity of the chromophore, locked in place by a H-bond to a water molecule. If Ile146's side chain occupied the same position in ECFP as Asn146 in GFP, the protein would be destabilized due to a less favorable solvation. Energy minimization during protein folding potentially leads to a twist of the seventh β-strand that buries Ile146 in the interior of the protein, whereas Tyr145, thanks to its partial hydrophilic character, reorients toward the bulk solvent (Figure 7a) and is stabilized by H-bonds to two waters of the protein's first hydration shell. The new conformation of residues [143−150] modifies the number and nature of the interactions of the chromophore with the protein; in particular, Ile146 and His148 are brought within VdW interaction distance of the indole ring of Trp66 from the chromophore. Indeed, our molecular dynamics simulations show that Trp66, Ile146, and His148 are engaged in VdW interactions and are likely to play a fundamental role in the fluorescence properties of ECFP (Table 3).

When considering the improvement of Cerulean versus ECFP, we first checked the importance of the S72A mutation that is known to improve folding efficiency (*2*). We did not observe any detectable difference between the spectroscopic properties of

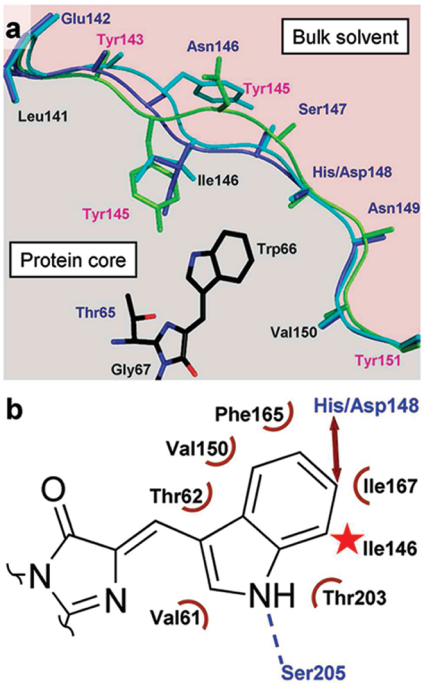

FIGURE 7: (a) Comparison of the interaction of the chromophore with the [143−150] strand in EGFP, ECFP, and Cerulean. Side chains are truncated to their C_β positions, except for residues 145 and 146. Names of hydrophobic and hydrophilic residues are colored black and blue, respectively. Tyrosines, because of their partial hydrophilic character, have purple names. The chromophore is colored black. Hydrophobic residues are all directed toward the interior of the protein. Hydrophilic residues are either parallel to or pointing outside the protein surface. This scheme illustrates the impact of the hydrophilic to hydrophobic N146I mutation between EGFP and ECFP/Cerulean and also shows that the strand enters deeper into the protein's core in the *cerulean* conformation than in the *ecfp* one. (b) Schematic representation of the interactions controlling the fluorescence properties of the chromophore in ECFP and Cerulean. The chromophore is stabilized by neighboring residues through van der Waals interactions (half-circles) and one H-bond (dashed line). The interaction that could affect chromophore planarity is represented as a double arrow, whereas the possible collisional quenching of chromophore fluorescence by Ile146 is shown by a red star. Hydrophilic residues and polar interactions are colored blue; hydrophobic residues and VdW interactions are colored black and brown, respectively.

ECFP-Y145A/H148D and those of Cerulean (Table 1), and their structures are almost identical (data not shown). However, we observed a clear effect of the mutation in our unfolding experiments aimed at measuring T_m and EC. The T_m of Cerulean is increased by 3.3 °C compared to that of ECFP-Y145A/H148D, and whereas the latter is almost immediately unfolded by 0.5 M NaOH, it takes 3 min to obtain a fully solvent exposed chromophore in Cerulean. This result is counterintuitive because the mutation essentially results in the replacement of an ~20 kJ/mol H-bond between Ser72 and Glu69, which is located on the helix bearing the chromophore, by a set of VdW interactions in Cerulean involving Ala72, Ile201, and Val224 with a total energy of only ~5 kJ/mol. Nevertheless, examination of the MD trajectories shows that this H-bond is transiently disrupted, suggesting that it does not have a strong stabilizing role in the central helix. Consequently, it appears likely that the S72A mutation plays a role only in the conformational energy landscape during protein folding and unfolding, events that we cannot probe in our experiments.

The comparison of the [143−150] strand position in ECFP and Cerulean highlights the role of the Y145A mutation. In ECFP, we have observed two conformations, *ecfp* and *ecfp′*, that differ by only four residues; in Cerulean, we observe the *ecfp* conformation and a new one, *cerulean*, in which the strand penetrates deeper into the protein. During the MD simulation, ECFP adopts a transient new conformation, *ecfp″*, which shares similarities with the *ecfp* (for the position of the strand main chain) and *cerulean* conformations (for the orientation of Ile146's side chain). Examination of the trajectory shows that the hydroxyl group of Tyr145 is constantly H-bonded to water molecules of the solvent. In Cerulean, Ala145 cannot be solvated in the same way; hence, the Y145A mutation likely favors the presence of the stable *cerulean* conformation which brings the main chain closer to the chromophore.

It has already been postulated that structural heterogeneity of the [143−150] strand has implications for the complex spectroscopic behavior of ECFP (*7*). We have now excluded the possibility that it is responsible for the two peaks in the absorption and fluorescence spectra. However, it is very likely that this structural heterogeneity, which is conserved in ECFP and Cerulean, is responsible for their complex fluorescence lifetime behaviors. Although Cerulean has primarily been assumed to be much improved in terms of monoexponential fluorescence decay, it has essentially two components, which is already an improvement when compared to ECFP (*10*, *11*). Given that the [143−150] strand can significantly alter its position on the 1−10 ns time scale (Figures 2 and 3), it is likely that it can interact with the chromophore in its excited state, for instance, through collision with Ile146. In the extreme case, it is possible that a molecule from the bulk solvent could occasionally enter the chromophore cavity and interact with the chromophore. It is conceivable that these interactions may eventually result in fluorescence quenching through vibrational energy dissipation. Our structural analysis provides a framework for analyzing the complexity of the fluorescence lifetime behavior of these tryptophan-based fluorescent proteins.

The low-pH structure of Cerulean raised questions about the configuration of the chromophore at physiological pH (*12*). Our results are unambiguous and uncover the structural response of Cerulean to a neutral−low pH transition (Figures S7 and S8 of the Supporting Information). *E*/*Z* isomerization of the chromophore around the C_β−C_γ bond probably happens at physiological pH as an infrequent event. Upon acidification, the solvent-exposed residue Asp148 becomes protonated and provides a stabilizing interaction to the $N_{\varepsilon 1}$ atom of the isomerized chromophore. The dynamics of the [143−150] strand is altered, and it adopts a new conformation, intermediate between the *ecfp* and *cerulean* conformations. Because of the different environment, residues from the chromophore cavity must reorganize. This constitutes a pH switch, by which the protein can maintain a certain level of fluorescence over a wide pH range. The long time scale (hours) of the spectroscopic conversion (*12*) underlines the infrequency of the isomerization. Certain fluorescent proteins homologous to GFP (e.g., highlighter fluorescent proteins) undergo reversible photoinduced off-switching of their fluorescence, and *E*/*Z* isomerization of the chromophore has been proposed to be involved in this transition between bright and dark states (*32*−*35*). In Cerulean, both configurations of the chromophore are planar and stabilized thanks to significant structural rearrangement, which supports the proposal that failure to accommodate the isomerized chromophore in an unprotonated planar conformation by the protein matrix is responsible for off-switching of highlighter fluorescent

proteins (*36*). Finally, pH-induced *E*/*Z* isomerization has also been observed for the red fluorescent proteins mKate (*37*) and mKeima (*38*).

After having identified structural differences between ECFP and Cerulean, we can try to explain why Cerulean exhibits an improved QY compared to that of ECFP. First, interactions between the chromophore and the surrounding residues control the planarity of the chromophore. It is widely accepted that everything else being equal, a more planar chromophore will have a better QY (Table 2) (*29*). The combination of our crystallographic and molecular dynamics data shows that the chromophore is indeed more planar in Cerulean, although the difference in planarity between the two proteins is higher in the simulation than in the experimental structures. We postulate that this difference originates from the glassy ice environment in the crystal at 100 K exerting a constraint on the [143−150] strand that is stronger than in the liquid environment at 300 K modeled in our simulation. Indeed, we observe that distances between this strand and the chromophore are consistently 0.2 Å shorter in the X-ray structures for this strand. In ECFP, Ile146 interacts with His148, which brings the latter residue within interaction distance of Trp66 and leads to the twisting of the indole ring relative to the rest of the chromophore. In contrast, Ile146 hardly interacts with Asp148 in Cerulean and the energy term between Asp148 and Trp66 is highly repulsive (Table 3). This demonstrates that the H148D mutation in Cerulean removes the interaction between residue 148 and the chromophore, allowing it to adopt a fully planar conformation.

Stabilization of the chromophore within the protein matrix favors radiative de-excitation pathways. The precise packing of amino acids against the chromophore plays a significant role in that regard. Besides residue 148, the only difference in the chromophore environment between ECFP and Cerulean resides in the closer positioning of Ile146 in one of the Cerulean conformers (Figure 4). In this conformation, Ile146 can contribute to the stabilization of the chromophore through VdW interactions via atoms $C_{\gamma 2}$ and $C_{\delta 1}$ (Figure 3). It appears that Ile146 rarely adopts this conformation in ECFP as it is not identifiable in the X-ray structure. Indeed, our molecular dynamics simulation shows that Ile146 interacts with His148 during most of the simulation [except when the side chain of His148 reorientates toward the solvent (see Movie S1)], thus hindering reorientation of its side chain toward the chromophore. This interaction is absent in Cerulean. Moreover, in the *cerulean* conformation, Ile146 establishes VdW interactions with Val61, Thr203, and Ile167, thereby filling a void in the vicinity of the chromophore (Figure 5). Calculation of the VdW interaction energy shows that the interaction between the four residues is favorable in that conformation (Table 3) and that they form a layer of atoms on one side of the chromophore that rigidifies its environment. We checked whether this would affect fluctuations of the Φ_i angles, thereby suggesting restriction of rotational movements of the chromophore as a reason for improvement of the QY (*39*). Since we did not observe noticeable differences in these fluctuations (Table 3), we specifically looked at the interaction between Ile146 and the chromophore and observed that a strong and stabilizing interaction was favored in the *cerulean* conformation of Cerulean, as well as in the infrequent *ecfp″* conformation of ECFP. By contrast, this interaction is repeatedly destabilizing ($E > 0$) in the *ecfp* conformation of both proteins (Figure 3d,e). This can be interpreted as follows. In the *cerulean*/*ecfp″* conformation, Ile146 "breathes" in a concerted manner with the chromophore, thanks to its strong interaction with Val61, Thr203, and Ile167. The change to the *ecfp* conformation drastically weakens the coupling between its movements and those of the chromophore, and Ile146 may then act as a potential quencher of the chromophore's excited state through collision events, although the efficiency of such a mechanism is yet to be evaluated. Evidently, the orientation of Ile146's side chain is controlled by the dynamics of the [143−150] strand, which implies that the improvement is only intermittent (Figure 6).

A more planar and better packed chromophore experiencing less collisional quenching constitutes a reasonable explanation for the better QY of Cerulean compared to that of ECFP (Figure 7b). Obviously, the QY could be higher if the [143−150] strand did not transiently adopt the *ecfp* conformation. We should realize that the chromophore cavity has been optimized by nature for a tyrosine-based chromophore, which is symmetric, and stabilized by H-bonds to the hydroxyl group on the symmetry axis. For the tryptophan-based chromophore, the polar atom nitrogen is off the symmetry axis of the molecule and can form a H-bond with only Ser205, leaving a large surface that can be stabilized through only VdW interactions. The engineering of such interactions is obviously more complicated than that of H-bonds.

CONCLUSION

We have shown that the tryptophan-based chromophore forms a very dynamic ensemble with the [143−150] strand in the fluorescent proteins ECFP and Cerulean. VdW interactions among Ile146, residue 148, and the indole ring of the chromophore control its planarity and stabilization, thus modulating its fluorescence quantum yield. These data provides new insights to further improve the fluorescence properties of tryptophan-based fluorescent proteins. An ideal system would contain mutations that permanently stabilize Ile146 in contact with the chromophore.

ACKNOWLEDGMENT

We thank Stephen Adams, Philippe Carpentier, Juan Fontecilla-Camps, Dominique Madern, Eve de Rosny, Xiaokun Shu, Roger Tsien, and Martin Weik for fruitful discussions and/or technical help. We also thank the ESRF for providing beamtime, members of the ESRF macromolecular crystallography group for their continuous support, the PSB for its support (particularly the RoBioMol and Cryobench platforms), and the staff at CCRT-CEA for technical assistance.

SUPPORTING INFORMATION AVAILABLE

Additional text, crystallography data table, additional figures, MD simulation movies, and appendices. This material is available free of charge via the Internet at http://pubs.acs.org.

REFERENCES

1. Chalfie, M., Tu, Y., Euskirchen, G., Ward, W. W., and Prasher, D. C. (1994) Green fluorescent protein as a marker for gene expression. *Science 263*, 802–805.
2. Cubitt, A. B., Woollenweber, L. A., and Heim, R. (1999) Understanding structure-function relationships in the *Aequorea victoria* green fluorescent protein. *Methods Cell Biol. 58*, 19–30.
3. Tsien, R. Y. (1998) The green fluorescent protein. *Annu. Rev. Biochem. 67*, 509–544.
4. Shaner, N. C., Steinbach, P. A., and Tsien, R. Y. (2005) A guide to choosing fluorescent proteins. *Nat. Methods 2*, 905–909.
5. Borst, J. W., Hink, M. A., van Hoek, A., and Visser, A. J. (2005) Effects of refractive index and viscosity on fluorescence and anisot-

ropy decays of enhanced cyan and yellow fluorescent proteins. *J. Fluoresc. 15*, 153–160.
6. Nguyen, A. W., and Daugherty, P. S. (2005) Evolutionary optimization of fluorescent proteins for intracellular FRET. *Nat. Biotechnol. 23*, 355–360.
7. Hyun Bae, J., Rubini, M., Jung, G., Wiegand, G., Seifert, M. H., Azim, M. K., Kim, J. S., Zumbusch, A., Holak, T. A., Moroder, L., Huber, R., and Budisa, N. (2003) Expansion of the genetic code enables design of a novel "gold" class of green fluorescent proteins. *J. Mol. Biol. 328*, 1071–1081.
8. Seifert, M. H., Ksiazek, D., Azim, M. K., Smialowski, P., Budisa, N., and Holak, T. A. (2002) Slow exchange in the chromophore of a green fluorescent protein variant. *J. Am. Chem. Soc. 124*, 7932–7942.
9. Rizzo, M. A., Springer, G. H., Granada, B., and Piston, D. W. (2004) An improved cyan fluorescent protein variant useful for FRET. *Nat. Biotechnol. 22*, 445–449.
10. Kremers, G. J., Goedhart, J., van Munster, E. B., and Gadella, T. W., Jr. (2006) Cyan and yellow super fluorescent proteins with improved brightness, protein folding, and FRET Forster radius. *Biochemistry 45*, 6570–6580.
11. Villoing, A., Ridhoir, M., Cinquin, B., Erard, M., Alvarez, L., Vallverdu, G., Pernot, P., Grailhe, R., Merola, F., and Pasquier, H. (2008) Complex fluorescence of the cyan fluorescent protein: Comparisons with the H148D variant and consequences for quantitative cell imaging. *Biochemistry 47*, 12483–12492.
12. Malo, G. D., Pouwels, L. J., Wang, M., Weichsel, A., Montfort, W. R., Rizzo, M. A., Piston, D. W., and Wachter, R. M. (2007) X-ray structure of Cerulean GFP: A tryptophan-based chromophore useful for fluorescence lifetime imaging. *Biochemistry 46*, 9865–9873.
13. Studier, F. W., Rosenberg, A. H., Dunn, J. J., and Dubendorff, J. W. (1990) Use of T7 RNA polymerase to direct expression of cloned genes. *Methods Enzymol. 185*, 60–89.
14. Pantoliano, M. W., Petrella, E. C., Kwasnoski, J. D., Lobanov, V. S., Myslik, J., Graf, E., Carver, T., Asel, E., Springer, B. A., Lane, P., and Salemme, F. R. (2001) High-density miniaturized thermal shift assays as a general strategy for drug discovery. *J. Biomol. Screening 6*, 429–440.
15. Jain, R. K., and Ranganathan, R. (2004) Local complexity of amino acid interactions in a protein core. *Proc. Natl. Acad. Sci. U.S.A. 101*, 111–116.
16. Kabsch, W. (1993) Automatic processing of rotation diffraction data from crystals of internally unknown symmetry and cell constants. *J. Appl. Crystallogr. 26*, 795–800.
17. Murshudov, G. N., Vagin, A. A., and Dodson, E. J. (1997) Refinement of macromolecular structures by the maximum-likelihood method. *Acta Crystallogr. D53*, 240–255.
18. Ward, W. W. (1981) in Bioluminescence and Chemiluminescence: Basic Chemistry and Analytical Applications (Deluca, M., and McElroy, W., Eds.) pp 235−242, Academic Press, New York.
19. Royant, A., Carpentier, P., Ohana, J., McGeehan, J., Paetzold, B., Noirclerc-Savoye, M., Vernède, X., Adam, V., and Bourgeois, D. (2007) Advances in spectroscopic methods for biological crystals. 1. Fluorescence lifetime measurements. *J. Appl. Crystallogr. 40*, 1105–1112.
20. Field, M. J., Albe, M., Bret, C., Proust-De Martin, F., and Thomas, A. (2000) The Dynamo Library for Molecular Simulations using Hybrid Quantum Mechanical and Molecular Mechanical Potentials. *J. Comput. Chem. 21*, 1088–1100.
21. Jorgensen, W. L., Maxwell, D. S., and TiradoRives, J. (1996) Development and testing of the OPLS all-atom force field on conformational energetics and properties of organic liquids. *J. Am. Chem. Soc. 118*, 11225–11236.
22. Jorgensen, W. L., Chandrasekhar, J., Madura, J. D., Impey, R. W., and Klein, M. L. (1983) Comparison of simple potential functions for simulating liquid water. *J. Chem. Phys. 79*, 926–935.
23. Demachy, I., Ridard, J., Laguitton-Pasquier, H., Durnerin, E., Vallverdu, G., Archirel, P., and Levy, B. (2005) Cyan fluorescent protein: Molecular dynamics, simulations, and electronic absorption spectrum. *J. Phys. Chem. B 109*, 24121–24133.
24. Antosiewicz, J., McCammon, J. A., and Gilson, M. K. (1994) Prediction of pH-dependent properties of proteins. *J. Mol. Biol. 238*, 415–436.
25. Senn, H. M., and Thiel, W. (2009) QM/MM Methods for Biomolecular Systems. *Angew. Chem., Int. Ed. 48*, 1198–1229.
26. Repasky, M. P., Chandrasekhar, J., and Jorgensen, W. L. (2002) Improved semiempirical heats of formation through the use of bond and group equivalents. *J. Comput. Chem. 23*, 1601–1622.
27. Suhling, K., Siegel, J., Phillips, D., French, P. M., Leveque-Fort, S., Webb, S. E., and Davis, D. M. (2002) Imaging the environment of green fluorescent protein. *Biophys. J. 83*, 3589–3595.
28. Voros, J. (2004) The density and refractive index of adsorbing protein layers. *Biophys. J. 87*, 553–561.
29. Shu, X., Shaner, N. C., Yarbrough, C. A., Tsien, R. Y., and Remington, S. J. (2006) Novel chromophores and buried charges control color in mFruits. *Biochemistry 45*, 9639–9647.
30. Shaner, N. C., Campbell, R. E., Steinbach, P. A., Giepmans, B. N., Palmer, A. E., and Tsien, R. Y. (2004) Improved monomeric red, orange and yellow fluorescent proteins derived from *Discosoma* sp. red fluorescent protein. *Nat. Biotechnol. 22*, 1567–1572.
31. Heim, R., and Tsien, R. Y. (1996) Engineering green fluorescent protein for improved brightness, longer wavelengths and fluorescence resonance energy transfer. *Curr. Biol. 6*, 178–182.
32. Andresen, M., Wahl, M. C., Stiel, A. C., Grater, F., Schafer, L. V., Trowitzsch, S., Weber, G., Eggeling, C., Grubmuller, H., Hell, S. W., and Jakobs, S. (2005) Structure and mechanism of the reversible photoswitch of a fluorescent protein. *Proc. Natl. Acad. Sci. U.S.A. 102*, 13070–13074.
33. Henderson, J. N., Ai, H. W., Campbell, R. E., and Remington, S. J. (2007) Structural basis for reversible photobleaching of a green fluorescent protein homologue. *Proc. Natl. Acad. Sci. U.S.A. 104*, 6672–6677.
34. Andresen, M., Stiel, A. C., Trowitzsch, S., Weber, G., Eggeling, C., Wahl, M. C., Hell, S. W., and Jakobs, S. (2007) Structural basis for reversible photoswitching in Dronpa. *Proc. Natl. Acad. Sci. U.S.A. 104*, 13005–13009.
35. Adam, V., Lelimousin, M., Boehme, S., Desfonds, G., Nienhaus, K., Field, M. J., Wiedenmann, J., McSweeney, S., Nienhaus, G. U., and Bourgeois, D. (2008) Structural characterization of IrisFP, an optical highlighter undergoing multiple photo-induced transformations. *Proc. Natl. Acad. Sci. U.S.A. 105*, 18343–18348.
36. Mizuno, H., Mal, T. K., Walchli, M., Kikuchi, A., Fukano, T., Ando, R., Jeyakanthan, J., Taka, J., Shiro, Y., Ikura, M., and Miyawaki, A. (2008) Light-dependent regulation of structural flexibility in a photochromic fluorescent protein. *Proc. Natl. Acad. Sci. U.S.A. 105*, 9227–9232.
37. Pletnev, S., Shcherbo, D., Chudakov, D. M., Pletneva, N., Merzlyak, E. M., Wlodawer, A., Dauter, Z., and Pletnev, V. (2008) A crystallographic study of bright far-red fluorescent protein mKate reveals pH-induced cis-trans isomerization of the chromophore. *J. Biol. Chem. 283*, 28980–28987.
38. Violot, S., Carpentier, P., Blanchoin, L., and Bourgeois, D. (2009) Reverse pH-dependence of chromophore protonation explains the large stokes shift of the red fluorescent protein mKeima. *J. Am. Chem. Soc. 131*, 10356–10357.
39. Megley, C. M., Dickson, L. A., Maddalo, S. L., Chandler, G. J., and Zimmer, M. (2009) Photophysics and dihedral freedom of the chromophore in yellow, blue, and green fluorescent protein. *J. Phys. Chem. B 113*, 302–308.